

Exact Wave Packet Dynamics of Singlet Fission in Unsubstituted and Substituted Polyene Chains within Long-Range Interacting Models

Suryoday Prodhana^{1, a)} and S. Ramasesha^{1, b)}

Solid State and Structural Chemistry Unit, Indian Institute of Science, Bangalore 560012, India

(Dated: 9 December 2024)

Singlet fission is a potential pathway for significant enhancement of efficiency in organic solar cells. In this article, we have studied singlet fission in a pair of polyene molecules employing exact many-body wave packet dynamics. The individual molecules are treated within Hubbard and Pariser-Parr-Pople (PPP) models and the interaction between them involves transfer terms, intersite electron repulsions and site charge-bond charge repulsion terms. Initial wave packet is constructed from excited singlet state of one molecule and ground state of the other. Time development of this wave packet under the influence of intermolecular interactions is followed within the Schrödinger picture by an efficient predictor-corrector scheme. In unsubstituted Hubbard and PPP chains, 2^1A excited singlet state leads to significant fission yield while the 1^1B state gives negligible fission yield. On substitution by donor-acceptor groups of moderate strength, singlet state derived from 1^1B state also gives significant fission yield within PPP model. Furthermore, we find the fission yield depends considerably on the stacking arrangement of the polyene molecules.

PACS numbers: 31.10.+z, 31.15.-p, 34.10.+x

Keywords: Singlet fission; Exact wave packet dynamics; Polyenes; Strongly correlated electronic systems.

I. INTRODUCTION

Photovoltaic cells are potential candidates in the field of “Green energy”, although their efficiencies are bounded by the Shockley-Queisser limit of 33% for a single layer p-n junction cell¹. There have been efforts to breach the upper bound by using different paradigms such as employing multiple p-n junction layers; by photon upconversion to harness sub-band gap radiation; by hot electron capture to reduce operating temperature of solar cell; and multiple exciton generation through absorption of a single high-energy photon. Multiple exciton generation on dissociation produces more than one electron and one hole per photon and can be envisaged in molecules if the absorbed photon energy is at least twice the energy of an appropriate lower energy excited state of the molecule. In semiconducting materials, the energy of the generated exciton should be at least twice of the band gap. In inorganic solar cells, quantum dots are found to be potential candidates for exploiting all of the above², while in organic solar cells, there has been intense effort to resort to singlet fission (SF) for enhancing the number of charge carriers produced per absorbed photon. Although this process has been known for a long time³, interest in exploiting it for higher efficiency organic solar cells is only a decade old and surfaced because of the ease of material processing and higher lifetime of triplet excitons⁴, leading to longer exciton diffusion length. Pursuit of systems with better SF efficiency beckons in-depth understanding of the mechanism which may lead to theoretical guide-

lines for the realization of new molecular systems.

Singlet fission is a process in which a molecule in the singlet excited state (S_n) interacts with another molecule in the ground state (S_0) resulting in triplet excited state on each molecule. Although this process can be described by a single step reversible pathway, a detailed scheme⁵ considering the hypotheses of spin-allowed transition is vividly accepted by the scientific community. In this scheme, interaction between the S_n state and S_0 state results in a spin-singlet coupled $^1(T_1T_1)$ state which later dissociates into two triplet excitons (Ref. 6–8 and references therein). Recently it has been reported that this multiexciton state being observed experimentally via time-resolved two-photon photoemission spectroscopy⁹ and transient absorption and time-resolved photoluminescence spectroscopy¹⁰. These studies also have shown more than 100% triplet yield from singlet excited state. In promising systems the rate constants for the fission of the singlet excited state should be higher, compared to other intra- and intermolecular processes like fluorescence. The energetics for singlet fission consists of two requirements- (i) $E_{S_n} \geq 2E_{T_1}$; systems with E_{S_n} slightly less than $2E_{T_1}$, have also been found to display signature of singlet fission due to vibronic processes (ii) the energy of the higher triplet state (T_2) should be greater than S_n energy to prevent intersystem crossing to the triplet state and also should be more than twice of T_1 energy to suppress re-fusion of the newly born triplets by triplet-triplet annihilation. In literature, S_1 which is the lowest singlet excited state is commonly considered to be the optically excited state. Michl and coworkers proposed a number of suitable SF candidates which satisfy the energetics criteria on the basis of single CI calculations within Pariser-Parr-Pople model¹¹ and speculated that alternant hydrocarbons (notably polyacenes)

^{a)} Electronic mail: suryodayp@sscu.iisc.ernet.in

^{b)} Electronic mail: ramasesh@sscu.iisc.ernet.in

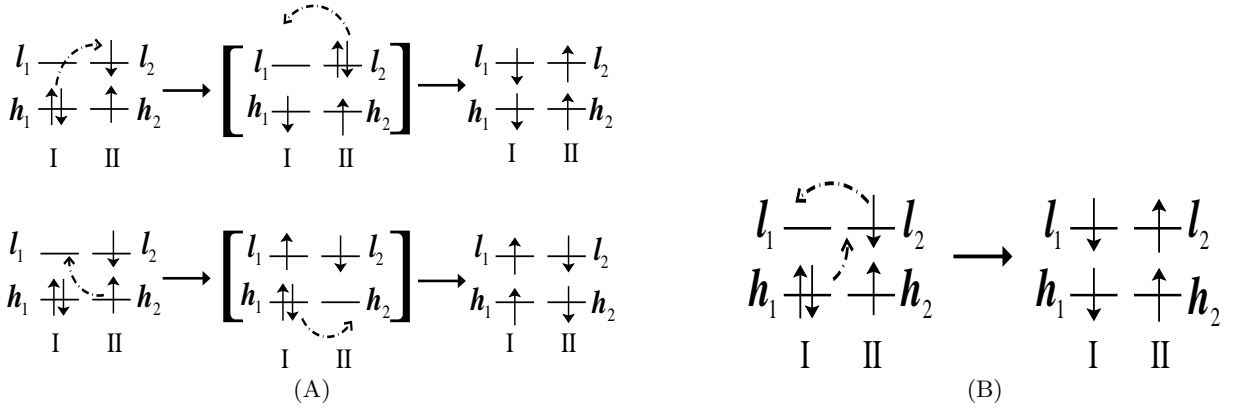


FIG. 1. (A) Schematic diagram of pathways for singlet fission involving two one-electron hopping interactions. h_1 and l_1 are the HOMO and LUMO of molecule 1 while h_2 and l_2 are those of molecule 2. The Hermitian conjugate of each step can be represented by reversing the direction of the broken arrow. (B) Schematic diagram of a pathway via two-electron repulsion integral involving three orbitals in a two-level system. Corresponding two-electron operators are $[l_1 l_2 | l_2 h_1](\hat{E}_{l_1 l_2} \hat{E}_{l_2 h_1} - \hat{E}_{l_1 h_1})$, $[l_1 l_2 | h_1 l_2] \hat{E}_{l_1 l_2} \hat{E}_{h_1 l_2}$, $[l_2 l_1 | l_2 h_1] \hat{E}_{l_2 l_1} \hat{E}_{l_2 h_1}$, $[l_2 l_1 | h_1 l_2] \hat{E}_{l_2 l_1} \hat{E}_{h_1 l_2}$ and their Hermitian conjugates, where \hat{E}_{ij} represents $\sum_{\sigma} \hat{a}_{i,\sigma}^{\dagger} \hat{a}_{j,\sigma}$.

and biradicaloids are good choices as chromophores for SF. In another study, Greyson and coworkers examined the appropriate strength of interchromophoric coupling necessary for singlet fission in some promising materials, employing density functional theory (DFT)¹².

Minami and Nakano gave a biradical description of singlet fission considering biradicaloid systems which have open-shell ground states¹³. They studied ordering and positioning of different excited states in a model H_4 system with variation in the multiple biradical character of the ground state. The description of the energy states are given in terms of frontier natural orbitals and it is predicted that singlet fission energy requirements along with better energy efficiency are best fulfilled by molecules having low or intermediate biradical character in their ground state. In this oversimplified picture, the electron-electron interactions are not considered beyond mean field description. They have also studied small-size oligorylenes¹⁴ and alternant and non-alternant hydrocarbons¹⁵ as singlet fission candidates employing the time-dependent density functional theory (TD-DFT). The notion that both lowest singlet excited state and lowest triplet state can be described by HOMO-LUMO excitations from the ground state is too crude for π -conjugated systems.

The spin-singlet coupled $^1(T_1 T_1)$ state can result from the singlet excited state either through a charge transfer intermediate pathway or via direct coupling between the initial state $S_0 S_1$ and final state $^1(T_1 T_1)$ through electron-electron interaction^{6,8}. The processes described can be understood within a two level picture of individual molecules. Let h_1 and l_1 be the HOMO and LUMO of molecule 1 and h_2 and l_2 are of molecule 2 respectively. The excited singlet state of one molecule in the proximity of the ground state of another is shown in Fig. 1. To create a triplet excited state on each molecule, such that the total $S_z = 0$ for the whole system, we can consider two pathways. Pathway 1 is a sequence of

two one-electron processes, which can be effected by the transfer (or resonance) integrals. One-electron transfer of the type $t_1 \hat{a}_{l_2 \uparrow}^{\dagger} \hat{a}_{h_1 \uparrow}$, where t_1 is the integral $\int \phi_{l_2}^* H' \phi_{h_1} d\tau$, H' being the interaction Hamiltonian results in the intermediate state (Fig. 1(A)); a next interaction through $t_2 \hat{a}_{l_1 \downarrow}^{\dagger} \hat{a}_{l_2 \downarrow}$ results in the final state with molecule 1 in $S = 1$, $S_z = -1$ state and molecule 2 in $S = 1$, $S_z = +1$ state. This two-step process can also proceed through $t'_1 \hat{a}_{l_1 \uparrow}^{\dagger} \hat{a}_{h_2 \uparrow}$ followed by $t'_2 \hat{a}_{h_2 \downarrow}^{\dagger} \hat{a}_{h_1 \downarrow}$. Of course the Hamiltonian also contains the corresponding Hermitian conjugates. The cross-section for each of the above mentioned processes can be crudely computed using Fermi Golden rule. The cross-section for singlet fission in any one of the channels of pathway 1 will be the product of the cross sections of the two processes in that pathway while the total cross-section will be the sum of the two pathways shown in Fig. 1(A). We can also conceive of a two-electron process by which the molecules in S_0 and S_1 can interact to give rise to two triplets (pathway 2). The two-electron integral $[l_1 l_2 | l_2 h_1]$ (in charge cloud notation) and its counterparts mentioned in the caption of Fig. 1(B) leads to the formation of two triplets.

However, the mechanism of $S_0 S_1 \rightarrow ^1(T_1 T_1)$ conversion has provoked quite a bit of debate. Michl and coworkers suggested that the direct coupling element $\langle S_0 S_1 | H_{inter} | ^1(T_1 T_1) \rangle$ for organic chromophores would be negligible and a virtual charge transfer intermediate is essential^{6,8}. Greyson et al. examined the above pathway with a charge transfer state intermediate within a model system of coupled chromophores and studied the effects of different factors like rate of decay, electronic coupling and the position of different eigenstates on the quantum yield, using DFT coupled with a density matrix approach to study dynamics¹⁶. Teichen and Eaves studied non-Markovian dynamics of electronic population transfer in a model dimer system assuming the presence of charge transfer intermediate state in the reaction pathway¹⁷.

Berkelbach et al. and D. Casanova put forward superexchange mediated pathway for S_0S_1 to $^1(T_1T_1)$ transformation in tetracene and pentacene dimers^{18,19}; charge transfer states participate in the coupling between S_0S_1 and $^1(T_1T_1)$ through second-order perturbative contributions. Beljonne et al. proposed an one-step mechanism for S_0S_1 to $^1(T_1T_1)$ transition within Davydov excitonic picture²⁰. On the other hand, Zimmerman et al. proposed a direct channel for SF in tetracene and pentacene crystals via non-adiabatic coupling^{4,21,22}. In this proposed mechanism, which is devoid of any charge transfer excitonic state, effective nuclear dynamics induces rapid population transfer from S_0S_1 state to the dark $^1(T_1T_1)$ state; this is followed by rapid separation of the two monomers in triplet state ($T_1 + T_1$). This direct coupling picture without any mediator has been supported by a number of other theoretical and experimental studies^{23–25}; Krylov et al. computed the relevant non-Markovian coupling term employing one-particle transition density matrix^{26,27} while Bardeen and coworkers proposed a direct spin-interaction based mechanism for this transition^{28–30}. A third viewpoint of SF mechanism has come forward recently on the basis of experimental observations which speculates quantum coherence between initial excited state and final multiexcitonic state^{9,31–33}; simultaneous population rise of both S_0S_1 and $^1(T_1T_1)$ states indicates quantum superposition of the respective states which has also been verified by DFT calculations.

Effect of crystal stacking on SF efficiency have been studied quite vividly for acenes and other hydrocarbons^{26,34–37}. In most of the materials, slipped stacked arrangement results in higher singlet fission yield as intermolecular vibrational modes which lead to direct coupling between the S_0S_1 state and $^1(T_1T_1)$ state are sensitive to crystal packing. However, reports by Friend et al. and Guldi et al. on solution phase SF for substituted pentacene pointed out that SF is not confined to specific geometries and can be observed even in disordered systems^{38,39}. Similar conclusion is also arrived at by Steigerwald and coworkers who studied SF of bipentacene in solution phase⁴⁰.

While there is a huge number of singlet fission studies reported (predominantly on acenes and other related systems), most of them are within a simplified picture of frontier molecular orbitals (FMO) of a pair of chromophores. These FMOs are determined either by simple self-consistent field calculations or via density functional theory. Within this FMO description, different relevant excited states are obtained either by simple HOMO to LUMO excitations (which is a crude approximation) or by time-dependent counterpart of DFT. However, the multiexcitonic state ($^1(T_1T_1)$) is a doubly excited state which is very poorly described within TD-DFT scheme^{41,42}. Additionally, as TD-DFT is devoid of proper functionals for deriving excited state energies correctly, the results obtained are not beyond doubt. Furthermore, most chromophores studied are π -conjugated

systems, where electronic correlation plays a strong role. There are only a few quantum mechanical studies reported which have considered higher order configuration interactions^{41–43}.

In this paper, we have gone beyond the static quantum chemical approach and studied the quantum dynamics of singlet fission. We have considered dimers of 1,3-butadiene, 1,3,5-hexatriene and 1,3,5,7-octatetraene in full configuration interaction space of the π -system within Hubbard and Pariser-Parr-Pople (PPP) model Hamiltonians. The polyene systems are important model molecules and there are several reports which indicate singlet fission in carotenoids and polyene systems^{43–49}. We start with a wave packet formed from the ground state of one molecule and the singlet excited state of another, these states being the exact eigenstates of the molecule within the chosen model Hamiltonians. We then introduce intermolecular interactions and evolve the wave packet in time. At each time step, the evolved wave packet is projected on to various direct products of the eigenstates of individual molecules in the triplet manifold to obtain the yield of the triplets. The time evolution is carried out in the full configuration space of the total π -system.

The S_1 states in these polyenes are optically inactive and are primarily composed of two triplets^{50,51}. Substitution in these moieties by donor-acceptor groups breaks the electron-hole and inversion symmetries making S_1 state optically active and therefore the lowest optical state in these systems shifts from S_2 to S_1 . However, for weak symmetry breaking S_1 state continues to show the characteristics of two triplets. Thus we find that even in substituted polyenes, if the initial state is an S_1 state rather than other higher energy singlet state, SF is efficient. This agrees with some recent studies which suggest substitution by heteroatoms within organic chromophore^{16,52,53} or copolymerising donor-acceptor moieties⁵⁴ can play an important role in tailoring candidate molecules for SF. Although we have not examined the dissociation of the coupled triplets in the later process, this model study will be helpful in understanding the underlying mechanism needed to develop better chromophores.

In the following section, we have given a brief account of the model Hamiltonians and methodology used in our study. In section III, we have discussed the pictures which emerge for unsubstituted polyenes within different model Hamiltonians along with the role of substitution in singlet fission yield for different alkene chain. In section IV, we summarize our study.

II. METHODOLOGY

We have sub-divided this into four subsections; in the first subsection, the model Hamiltonians of individual monomers are given. This is followed by the description of the Hamiltonian for the full system. In the third, we

have discussed the construction of the initial wave packet and the techniques employed for its time evolution. In the last subsection, methods for analyzing the evolved wave packet is presented.

A. Model Hamiltonians of Individual Monomers

In our study, the individual molecules considered are polyenes which have chain lengths, N varying from 4 to 8 sites. To study the role of substitution, site energies are varied at the chain ends to mimic donor and acceptor groups. Positive site energies correspond to donor groups and negative site energies to acceptor groups while site energies of unsubstituted carbon atoms are all set to zero. The model Hamiltonian employed is the Pariser-Parr-Pople (PPP) Hamiltonian^{55,56}, which includes long-range electron correlations along with on-site Hubbard interaction (U). The Hamiltonian of individual polyene is given by:

$$H_{intra} = \sum_{i=1}^{N-1} t_0 (1 - (-1)^i \delta) (\hat{E}_{i,i+1} + \text{H.C.}) + \sum_{i=1}^N \epsilon_i \hat{n}_i + \sum_{i=1}^N \frac{U}{2} \hat{n}_i (\hat{n}_i - 1) + \sum_{i>j=1}^N V_{ij} (\hat{n}_i - z_i) (\hat{n}_j - z_j) \quad (1)$$

$$\hat{E}_{i,i+1} = \sum_{\sigma} \hat{c}_{i,\sigma}^{\dagger} \hat{c}_{i+1,\sigma}$$

where t_0 is the average transfer integral; δ is the strength of dimerization; ϵ_i is the site energy at the i -th site; U is the Hubbard correlation strength and V_{ij} -s are the intersite electronic correlation strengths; z_i is the local chemical potential at site i which leaves the site neutral (for carbon in a π -conjugated system $z_i = 1$). $\hat{c}_{i,\sigma}^{\dagger}$ ($\hat{c}_{i,\sigma}$) creates (annihilates) an electron of spin σ in the orbital at i -th site and \hat{n}_i is the corresponding number operator. Standard PPP parameters for carbon are employed, namely $t_0 = -2.40$ eV and $U = 11.26$ eV while the strength of donor-acceptor substitution, $|\epsilon|$ is varied from 0 to 5 eV. δ is taken as 0.07 and the C-C bond lengths are fixed at $1.40(1 + \frac{\delta}{2})$ Å for the single bond and $1.40(1 - \frac{\delta}{2})$ Å for the double bond. The long-range Coulomb interaction term V_{ij} is parameterized using Ohno interpolation scheme⁵⁷.

If all long-range intersite interaction terms in the Hamiltonian are discarded, it represents Hubbard Hamiltonian. Singlet fission in unsubstituted systems are also studied within this model Hamiltonian, as a function of U/t_0 to probe the role of correlation strength. The $U/t_0 = 0$ case will reproduce the non-interacting Hückel picture. In both Hückel and Hubbard model, we have considered $t_0 = -1.0$ eV and the dimerization strength same as in the PPP model.

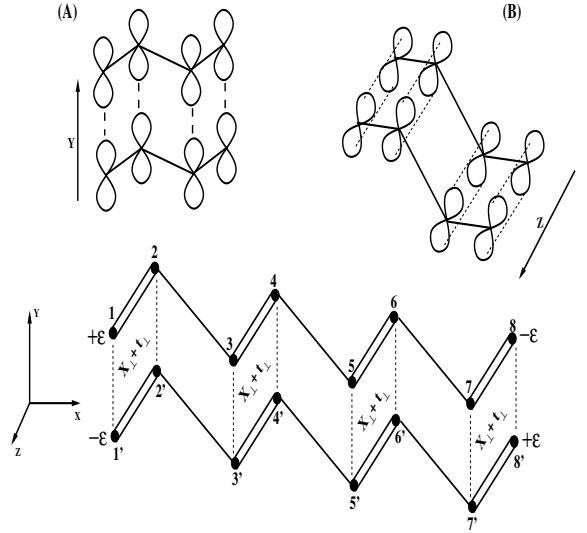


FIG. 2. Schematic diagram of the stacked polyenes; (A) in vertical stacking, monomers get stacked along Y-axis; (B) in horizontal stacking, monomers get stacked along Z-axis. XY plane is the molecular plane. The broken lines represent the intermolecular hopping interaction. $+\epsilon$ and $-\epsilon$ represent the donor and acceptor sites respectively while δ is the dimerization factor. The intrachain transfer integrals are taken to be $t_0(1 \pm \delta)$ for double/single bonds and corresponding bond lengths are taken to be $r_0(1 \mp \delta/2)$. t_0 and r_0 are chosen to be 2.40 eV and 1.4 Å respectively. Site indices on different molecules are differentiated by using ‘prime’ superscript for sites on one molecule and without ‘prime’ for the other molecule.

The above Hamiltonians, being non-relativistic conserves total spin S_{total} , along with z-component of total spin ($S_{z,total}$). As we are primarily concerned with singlet and triplet manifolds, we work with valence bond (VB) basis which are eigenstates of total spin and employ the diagrammatic valence bond (DVB) method^{58,59} for obtaining eigenstates in different spin subspaces for the monomers. Though complete and linearly independent, these basis states are non-orthogonal and result in non-symmetric sparse Hamiltonian matrices for the polyenes in question. The Hamiltonians are fully diagonalized in each case to obtain the complete spectrum within the singlet and triplet subspaces of individual polyenes.

B. Hamiltonian for Intermolecular Interactions

For probing singlet fission, we have considered two polyene monomers arranged in an eclipsed conformation with the separation between the two moieties set at 4 Å. The stacking orientation of the two monomers can be either “vertical” (V stacking), where one monomer remains on top of another or “horizontal” (H stacking), as shown in Fig. 2(A) and 2(B). In both orientations, these monomers remain in an electrostatically favorable stacking configuration where the donor (acceptor) site of molecule I lies directly above the acceptor (donor) site of molecule II (Fig. 2).

The intermolecular Hamiltonian between the two monomers is given by:

$$\begin{aligned}
H_{inter} = & \sum_{\langle i, i' \rangle} t_{\perp} (\hat{E}_{i, i'} + \hat{E}_{i', i}) \\
& + \sum_i \sum_{j'} V_{ij'} (\hat{n}_i - z_i) (\hat{n}_{j'} - z_{j'}) \\
& + \sum_{\langle i, i' \rangle} X_{\perp} (2\hat{n}_i + 2\hat{n}_{i'} - 2) (\hat{E}_{i, i'} + \hat{E}_{i', i})
\end{aligned} \quad (2)$$

where t_{\perp} is the inter-polyene hopping term between corresponding sites i and i' on chains I and II which are directly above each other (Fig. 2). The transfer term is negative for horizontal stacking while it is positive for vertical stacking due to opposite signs of the overlap integrals (Fig. 2); in our calculations, we have considered $|t_{\perp}| = 0.5$ eV in the PPP model and 0.2 eV within Hückel and Hubbard models. The electron repulsion term comparable to the inter-molecular transfer term is X_{\perp} , the site charge-bond charge repulsion term and represents the two-electron integral $[ii|ii']$ and other related integrals within the charge cloud notation (Ref. 60); the other relevant multielectron repulsion term, bond charge-bond charge repulsion, represented by $[ii'|ii']$, is neglected as it is expected to be much smaller compared to X_{\perp} (Ref. 61). The site charge-bond charge term is neglected in the intra-molecular Hamiltonian as it affects only weakly the excitation spectrum of the isolated molecule. We have also taken $X_{\perp} = 0$ for pair of sites on the two molecules which are not directly above each other. In charge cloud notation, the contribution to the Hamiltonian due to the repulsion term between site charge at i (of chain I) and the bond between i and i' (of chain II) can be denoted by the parameter $X_{\perp, \langle ii, ii' \rangle} = [ii|ii'] + [ii|i'i] + [i'i|i'i] + [i'i|ii]$; all integrals in this expression are equal and the corresponding second quantized operators are $(\hat{n}_i - 1)\hat{E}_{ii'}$, $\hat{n}_i\hat{E}_{i'i}$, $\hat{n}_{i'}\hat{E}_{ii'}$ and $(\hat{n}_{i'} - 1)\hat{E}_{i'i}$ respectively. Equivalent repulsion parameter $X_{\perp, \langle i'i', ii' \rangle}$ will also generate four interaction terms in the intermolecular Hamiltonian. In the non-interacting (Hückel) picture, X_{\perp} term is taken to be zero.

C. Initial Wave Packet Construction and Time Evolution

Dynamics of the time evolution of a wave packet, which is direct product of a specified excited singlet state S_n^I of monomer I and the ground state S_0^{II} of monomer II, is studied in the Schrödinger picture employing the full system Hamiltonian $H_{full} = H_{intra} + H_{inter}$. We have chosen the Schrödinger picture over the interaction picture as the full space of the dimer is too large to study within the interaction picture. It is convenient to obtain the eigenstates (both singlet and triplet) of the isolated molecules in the VB basis and convert them into Slater basis. The Hamiltonian matrix corresponding to H_{full} is generated in the Slater basis with $S_z^{full} = 0$. Evolution of the wave packet is accomplished by applying two

schemes which do not require the knowledge of complete eigenspectrum of the dimer moiety. The Crank-Nicholson (CN) scheme (Eq. 3) is an unitary and unconditionally stable scheme⁶², although the computational cost due to Hamiltonian matrix inversion at each step forces us to use this scheme only to initiate the time evolution. The CN scheme can be described by equating the forward time evolved wave packet from time t to $t + \Delta t/2$ to the backward time evolved wave packet from time $t + \Delta t$ to $t + \Delta t/2$, by forcing unitarity, i.e.

$$\begin{aligned}
(1 + iH_{full}\Delta t/2\hbar)|\psi(t + \Delta t)\rangle \\
= (1 - iH_{full}\Delta t/2\hbar)|\psi(t)\rangle + O((H_{full}\Delta t)^3)
\end{aligned} \quad (3)$$

This equation can be put in the form of a linear algebraic equation by using Slater basis of the full system with $S_z^{full} = 0$. The algebraic equation $A\vec{x} = \vec{b}$ is then defined by $A = (1 + iH_{full}\Delta t/2\hbar)$, $\vec{b} = (1 - iH_{full}\Delta t/2\hbar)|\psi(t)\rangle$ with $|\psi(t)\rangle = \sum_i c_i |i\rangle$. $\{|i\rangle\}$ is the Slater basis space of the full system and we wish to solve for \vec{x} which defines $|\psi(t + \Delta t)\rangle = \sum_i x_i |i\rangle$. The $|\psi(t + \Delta t)\rangle$ is calculated by inverting the matrix $(1 + iH_{full}\Delta t/2\hbar)$, which is done using a small matrix algorithm analogous to the Davidson scheme⁶³. These time evolved states, obtained by CN scheme for the first three time steps are further evolved over longer periods using fourth-order multistep differencing scheme (MSD4),

$$\begin{aligned}
|\psi(t + 2\Delta t)\rangle = |\psi(t - 2\Delta t)\rangle + \frac{4iH_{full}\Delta t}{3} \left[|\psi(t)\rangle \right. \\
\left. - 2(|\psi(t + \Delta t)\rangle + |\psi(t - \Delta t)\rangle) \right] + O((H_{full}\Delta t)^5)
\end{aligned} \quad (4)$$

introduced by Iitaka⁶⁴. It is an integrable and conditionally stable scheme which does not require matrix inversion and is accurate up to $(H_{full}\Delta t)^5$.

The result obtained is further improved by fourth-order Adams-Moulton scheme (Eq. 5).

$$\begin{aligned}
|\psi(t + 2\Delta t)\rangle = |\psi(t + \Delta t)\rangle - \frac{iH_{full}\Delta t}{24} \left[9|\psi(t + 2\Delta t)\rangle \right. \\
\left. + 19|\psi(t + \Delta t)\rangle - 5|\psi(t)\rangle + |\psi(t - \Delta t)\rangle \right]
\end{aligned} \quad (5)$$

This predictor-corrector scheme⁶⁵ (MSD4 scheme being the predictor and Adams-Moulton scheme the corrector) is found to be very robust with accuracy comparable to the CN scheme, with the added advantages of being faster and less memory intensive. The validity of the above scheme is also examined by comparing the time evolution of small systems, calculated by exact methods like either evolving the initial state using the matrix representation of $\exp(-iH_{full}\Delta t)$ or by projecting the initial state on the eigenstates of H_{full} and explicitly evolving these eigenstates using their corresponding eigenvalues.

The Hamiltonian matrix used for the largest system in our study (16 carbon atoms) is of dimension ~ 166

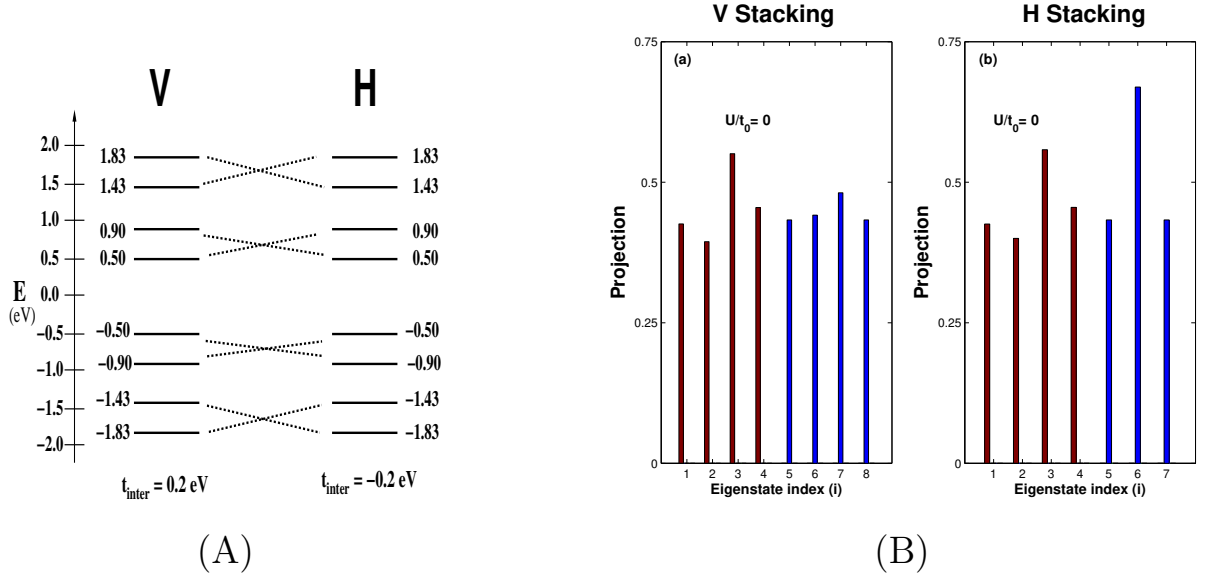


FIG. 3. (Color online) (A) Molecular orbitals of 1,3-butadiene dimer in V and H stackings. Correlation between the one-particles states in different stackings are shown by broken lines. (B) Indexing of the many-body eigenstates of the full system Hamiltonian with significant overlaps with $1^1B \otimes 1^1A$ (dark brown) and $T_1 \otimes T_1$ (dark blue). The stacking type is indicated by the letters V and H in both subfigures. Note that no eigenstates of H_{full} has significant overlap with both $1^1B \otimes 1^1A$ and $T_1 \otimes T_1$ simultaneously.

million and for reasonable convergence, Δt of the order of $0.002 \text{ eV} / \hbar$ is used for the PPP model, which is typically $\sim 0.00132 \text{ fs}$; for Hückel and Hubbard model, Δt is taken as $0.01 \text{ eV} / \hbar$ ($\sim 0.0066 \text{ fs}$). Hence, to follow the dynamics for just 30 fs , the time evolution has to be carried out for more than 20000 time steps within the PPP model and nearly 5000 time steps within the other two models.

D. Analysis of the Evolved Wave Packet

After each time evolution step, the evolved state is projected onto the desired direct product of the triplet eigenstates of I and II i.e. $T_m^I \otimes T_n^{II}$, where T_m and T_n are triplet eigenstates of individual monomers. The total S_z value of the wave packet remains unaltered during time evolution, hence, the projection on the triplet channel is carried out in the same S_z space; in this case, both monomers in the triplet state can have $S_z = 0$ or one of them has $S_z = +1(-1)$ while the other has $S_z = -1(+1)$. Triplet eigenstates of individual monomers are calculated in $S_z = +1$ space using VB basis and employing \hat{S}^- operator, corresponding eigenstates in $S_z = 0$ and -1 spaces are obtained. The yield in a given pair of triplet eigenstates (m, n) is given by $I_{m,n}(t) = |\langle \psi(t) | T_m^I \otimes T_n^{II} \rangle|^2$ where $|T_m^I \otimes T_n^{II}\rangle = \frac{1}{\sqrt{3}} |T_{m,S_z=0}^I \otimes T_{n,S_z=0}^{II}\rangle - \frac{1}{\sqrt{3}} [|T_{m,S_z=+1}^I \otimes T_{n,S_z=-1}^{II}\rangle + |T_{m,S_z=-1}^I \otimes T_{n,S_z=+1}^{II}\rangle]$, according to angular momentum algebra of generating a combined $S = 0$ object from two $S = 1$ objects. However, the number of such pairs for a neutral subsystem can be enormous; number of triplet-triplet channels for octatetraene is 5531904 as

each molecule has 2362 triplet states. Hence, the number of pairs to be investigated in each dimer system needs to be significantly reduced. This is achieved by restricting to ~ 10 low-lying triplet states on each of the neutral subsystems (corresponding to one hundred channels) and by applying a cut-off in the yield ($\sim 10^{-3}$), which a channel must have at least at one step during the course of the full evolution.

III. RESULTS AND DISCUSSION

Results of our study are presented in terms of the integrated yield over the time period of evolution, defined as $I_{m,n}^{total} = \sum_i I_{m,n}(t_i) \Delta t$, where $I_{m,n}(t_i)$ is the yield at i -th step in triplet pair channel (m, n) and Δt is the time gap. Higher value of total yield signifies greater probability of generating triplet excitons on dissociation of the evolved coupled state. The study we have undertaken is a non-dissipative study. Hence, we do observe some unphysical situations such as formation of final states with energies higher than the initial state ($m, n > 1$). We have also observed Rabi type oscillations⁶⁶ as expected from non-dissipative quantum dynamics. However, physically important final state is $T_1 \otimes T_1$ and we have focussed only on this state in all our further discussions. Since, we have considered only $I_{1,1}(t)$, the subscript is dropped in all later discussions.

In all the model calculations, we have considered two different scenarios about the nature of the S_n state. In scenario I, we have considered $S_n \equiv S_1$; i.e., the lowest energy singlet excited state of the monomer is employed in constructing the initial wave packet. In unsubstituted polyenes, this state remains in the same symmetry sub-

TABLE I. Dependence of total yield (I^{total}) on the parameters of H_{inter} in the Hubbard and PPP models for a pair of butadiene and hexatriene. For octatetraene, we have only reported Hubbard results. X_{\perp} is the site charge-bond charge repulsion term which is either zero or 0.2 eV for Hubbard model and 0.5 eV for PPP model. t_{\perp} is the intermolecular transfer term between corresponding sites and within Hubbard model in units of t_0 , $t_{\perp} = +0.2$ in V stacking and $t_{\perp} = -0.2$ in H stacking. In the PPP model, $t_{\perp} = 0.5$ eV in V stacking and $t_{\perp} = -0.5$ eV in H stacking.

System	Model	U/t_0	$X_{\perp} = 0$		$X_{\perp} \neq 0, t_{\perp} = 0$		$X_{\perp} \neq 0, t_{\perp} \neq 0$	
			V	H	V	H	V	H
butadiene	Hubbard	2.0	1.70	1.70	2.32	2.32	1.62	1.18
		4.0	0.66	0.66	2.45	2.45	2.90	0.30
		6.0	0.26	0.26	1.84	1.84	2.65	0.13
	PPP		4.54	4.55	4.29	4.01	3.30	3.94
hexatriene	Hubbard	2.0	2.47	2.47	2.01	2.01	0.86	1.91
		4.0	1.11	1.11	2.93	2.93	2.12	0.59
		6.0	0.64	0.64	2.47	2.47	3.21	0.35
	PPP		4.90	4.92	3.99	4.01	2.19	4.79
octatetraene	Hubbard	2.0	2.98	2.98	1.32	1.32	0.80	2.34
		4.0	2.13	2.13	3.18	3.18	1.84	1.47
		6.0	1.57	1.57	3.10	3.10	3.16	0.89
	PPP		—	—	—	—	1.92	6.04

space as the ground state for standard PPP parameters. On the other hand, in scenario II, the lowest optical state is considered as the S_n state ($S_n \equiv S_{op}$). Substitution by donor-acceptor groups at the end of the chains breaks spatial symmetry (C_2) as well as electron-hole symmetry and results in mixing of eigenstates of different symmetries of the unsubstituted system; consequently, every eigenstate becomes optically allowed on substitution. In this case, we have considered the state with highest transition dipole moment from the ground state (within an energy window) as S_{op} , i.e. $S_n \equiv S_{op} = S_{\mu_{tr}^{max}}$. In all substituted polyenes, it has been assumed that the donor and acceptor strengths are same, i.e. $|\epsilon_D| = |\epsilon_A| = \epsilon$. In each polyene system considered, for large enough ϵ , S_1 and S_{op} states become same and there remains no difference between the two scenarios.

In a simplified two-level picture, the probability of transition from initial state $|i\rangle$ to final state $|f\rangle$ under the influence of a time-independent perturbation V is,

$$|c_f|^2 = 2 \frac{|\langle i|V|f\rangle|^2}{(E_f - E_i)^2} [1 - \cos(\omega_{fi}t)] \quad (6)$$

In present study, the initial direct product state $|S_n\rangle \otimes |S_0\rangle$ can be assumed as $|i\rangle$ while the triplet-triplet channel $|T_1\rangle \otimes |T_1\rangle$ as the final state $|f\rangle$. If the oscillation term is neglected for the moment, the yield is proportional to square of the magnitude of the coupling matrix element $V_{i,f}$ and inversely proportional to the energy difference between these two states. At the zeroth level approximation, the energies of these coupled states can be approximated as the sum of individual monomer energies. For all polyene system studied, the coupling element $V_{i,f}$ is of the order of 10^{-20} , negligibly small, within PPP model

and zero in the other two models. Hence, the simple two-level description will not suffice for studying singlet fission in π -conjugated systems in general. However, two-level system gives valuable insights particularly when the states $|S_n\rangle \otimes |S_0\rangle$ and $|T_1\rangle \otimes |T_1\rangle$ are nearly degenerate. The states $|S_n\rangle \otimes |S_0\rangle$ and $|T_1\rangle \otimes |T_1\rangle$ are nearly degenerate in long unsubstituted polyenes when S_n corresponds to the lowest two-photon state and T_1 is the lowest triplet state. In this case, the nondegenerate perturbation theory breaks down. Within the time-independent degenerate perturbation theory, the perturbation term mixes the two states $|S_n\rangle \otimes |S_0\rangle$ and $|T_1\rangle \otimes |T_1\rangle$. Therefore, evolution of the initial wave packet results in large yield in the $|T_1\rangle \otimes |T_1\rangle$ channel.

The time evolution can be analyzed in more detail by focussing on the eigenstates of the full system. In this method, $I(t)$, the yield in $|T_1\rangle \otimes |T_1\rangle$ channel at a particular time-step t is given by,

$$\begin{aligned} |\langle T_1 \otimes T_1 | \Psi(t) \rangle|^2 &= \sum_i |\langle S_n \otimes S_0 | \psi_i(0) \rangle \langle T_1 \otimes T_1 | \psi_i(0) \rangle|^2 \\ &+ 2 \sum_i \sum_{j>i} \text{Re} \{ \langle S_n \otimes S_0 | \psi_i(0) \rangle \langle T_1 \otimes T_1 | \psi_i(0) \rangle \\ &\quad \langle \psi_j(0) | S_n \otimes S_0 \rangle \langle \psi_j(0) | T_1 \otimes T_1 \rangle \} \cos(\omega_{ij}t) \end{aligned} \quad (7)$$

$$\omega_{ij} \equiv (E_i - E_j)/\hbar$$

where $\Psi(t)$ is the time-evolved many-body state and $\{\psi_i(0)\}$ are the eigenstates of the full system Hamiltonian, H_{full} . From Eq. 7, it can be noted that for a high cross-section in singlet fission, it is necessary that

TABLE II. Full system eigenstates of 1,3-butadiene dimer having significant projections with $2^1A \otimes 1^1A$ (P_i) and $T_1 \otimes T_1$ (P_f) in the PPP model are tabulated for V and H stacking. When the lowest optical state is considered as the excited state of the initial wave packet, P_i corresponds to $\langle 1^1B \otimes 1^1A | \psi_i(0) \rangle$. E_k is the energy of the eigenstate ‘k’ as measured from the many-body ground state in eV.

Sr. No. (k)	V stacking								H stacking							
	2^1A				1^1B				2^1A				1^1B			
	E_k	P_i	P_f	$P_i \times P_f$	E_k	P_i	P_f	$P_i \times P_f$	E_k	P_i	P_f	$P_i \times P_f$	E_k	P_i	P_f	$P_i \times P_f$
1	3.15	0.3	0.7	0.2	3.15	0.0	0.7	0.0	5.15	0.3	0.9	0.3	5.15	0.0	0.9	0.0
2	5.18	0.6	0.4	0.2	3.71	0.6	0.0	0.0	5.35	0.6	0.4	0.2	5.33	0.6	0.0	0.0
3	6.82	0.2	0.1	0.02	5.18	0.0	0.4	0.0					5.35	0.0	0.4	0.0
4	8.34	0.1	0.3	0.03	5.62	0.5	0.0	0.0					5.67	0.6	0.0	0.0
5					5.73	0.4	0.0	0.0					7.81	0.3	0.0	0.0
6					8.01	0.2	0.0	0.0					7.92	0.3	0.0	0.0
7					8.34	0.005	0.3	0.001								
8					9.12	0.2	0.0	0.0								
9					9.50	0.2	0.008	0.001								

at least one of the eigenstates of the full system Hamiltonian has simultaneously large non-zero overlaps with the initial and final states. Additionally, the oscillating factor $\cos(\omega_{ij}t)$ also plays a role as it can both enhance or reduce $I(t_i)$. In our study, this particular analysis is employed only for the dimer of 1,3-butadiene; for longer polyene chains, calculating the complete eigenspace of the full system Hamiltonian is beyond present computational capacity.

We will discuss first the dynamics in the Hückel picture and proceed to Hubbard model in which only on-site interactions are considered. Finally we discuss the more realistic PPP model results.

1. Hückel Model

In the non-interacting picture, the lowest energy excited state is also the optical state ($S_1 \equiv 1^1B$). The two-photon state remains much higher in energy compared to the optical state and we do not consider evolution from this state. The energies of the lowest optical state and the lowest triplet state are same in the Hückel picture. Thus energetically a single optically excited molecule cannot yield two triplets in the Hückel model. Indeed, yields in the $T_1 - T_1$ channel are zero for both V and H stackings. On tuning t_\perp from +0.2 eV to -0.2 eV, the evolved molecular orbitals interchange their energies in pairs as shown in Fig. 3(A). The energy difference between the initial wave packet and the final coupled state, however, remain equal to t_0 . Besides, as shown in the histograms in Fig. 3(B), the overlap integrals of the full system eigenstates with the initial and final states are not large simultaneously, which is a prerequisite for large yield. Hence,

we can conjecture that without electronic correlations, the cross-section of singlet fission is negligible.

2. Hubbard Model

We have studied singlet fission for a pair of butadienes, hexatrienes and octatetraenes within the Hubbard model for different on-site correlation strength. In order to understand the role of X_\perp term vis a vis that of t_\perp , these systems have been studied when X_\perp is zero as well as when it is nonzero. We have studied these systems for different stackings (V and H), characterized by $t_\perp > 0$ and $t_\perp < 0$. In Table. I, we have presented the total yield of butadiene, hexatriene and octatetraene for $U/t_0 = 2, 4$ and 6. We have taken 2^1A state as the singlet excited state for constructing the initial wave packet. When the site charge-bond charge term is turned off, yields are same for both V and H stackings. The total yield also reduces with increasing U/t_0 and this trend can be seen for all three polyenes. This is because, larger U/t_0 suppresses contributions from ionic configurations in the wave packet while it is the ionic configurations which are intermediates for the final product. Larger $T_1 - T_1$ yield in longer systems is due to the higher number of intermolecular transfer terms that are operative.

For probing the importance of X_\perp term compared to the one-electron transfer term, we have also obtained I^{total} when t_\perp is taken to be zero with $X_\perp = 0.2$ eV (Table. I). Since $t_\perp = 0$, there is no difference between the V and H stackings in the Hubbard model. Interestingly, in this case total yields are much larger compared to $X_\perp = 0, t_\perp \neq 0$ case. Besides, I^{total} is highest for $U/t_0 = 4$ in all three polyenes which implies that when correlations are of intermediate strengths, the yields are highest. If the correlations are very weak, the energies of the initial and final states are very different while in strongly correlated systems, intermediate ionic configurations are

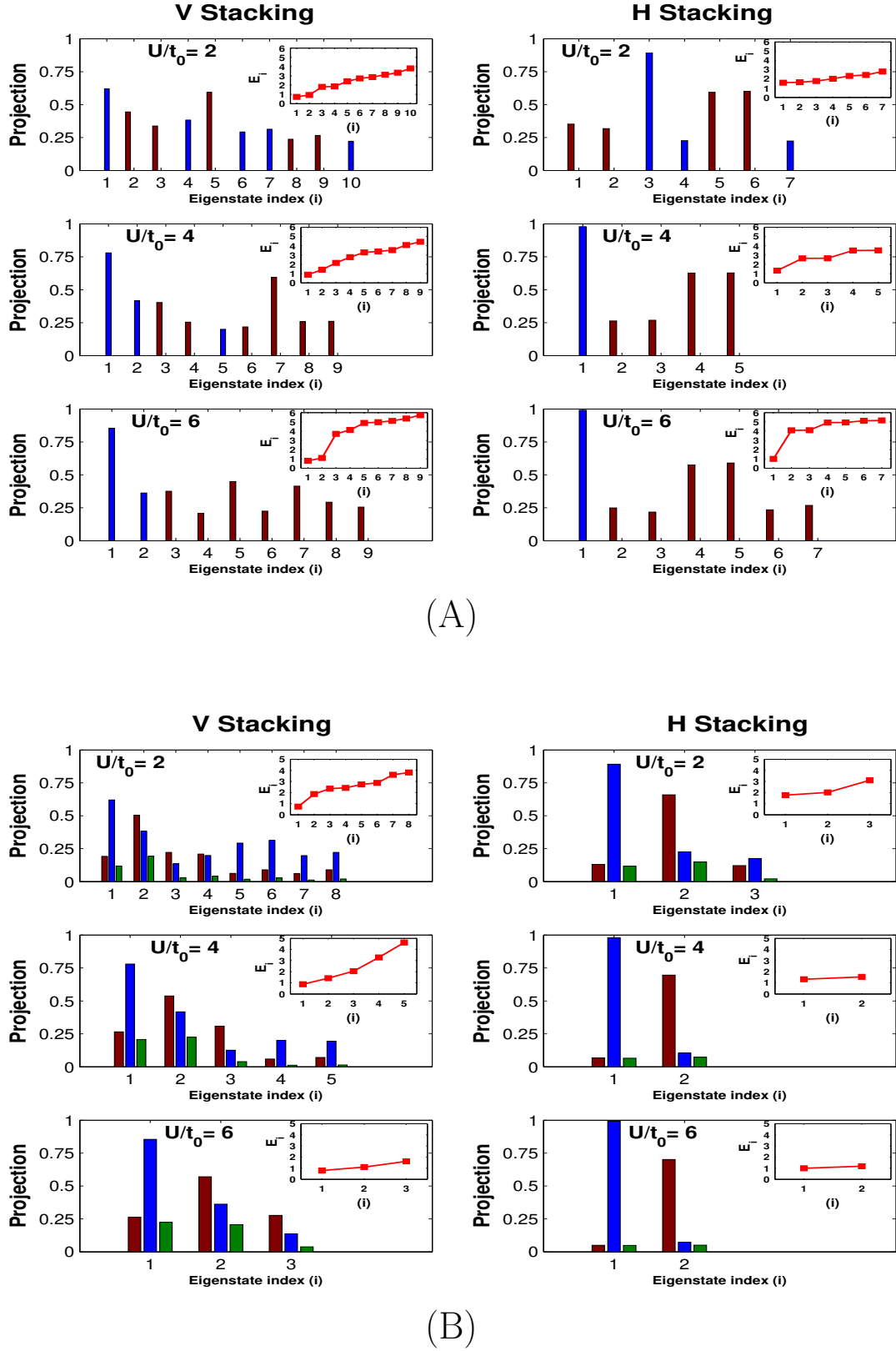


FIG. 4. (Color online) (A) Significant projections of $1^1B \otimes 1^1A$ and $T_1 \otimes T_1$ with eigenstates of the dimer system within Hubbard model are shown while in (B) significant projections of $2^1A \otimes 1^1A$ and $T_1 \otimes T_1$ with full system eigenstates are shown as histograms. In both (A) and (B), the left panel corresponds to V stacking while the right panel corresponds to H stacking. The color indices are as follows: dark brown, projection to initial state, $P_i \equiv \langle S_n \otimes S_0 | \psi_i \rangle$; dark blue, projection to final state, $P_f \equiv \langle T_1 \otimes T_1 | \psi_i \rangle$; dark green, $P_i \times P_f$. Inset: E_i , the energy of the significant eigenstate 'i' as measured from the ground state of the full system is shown.

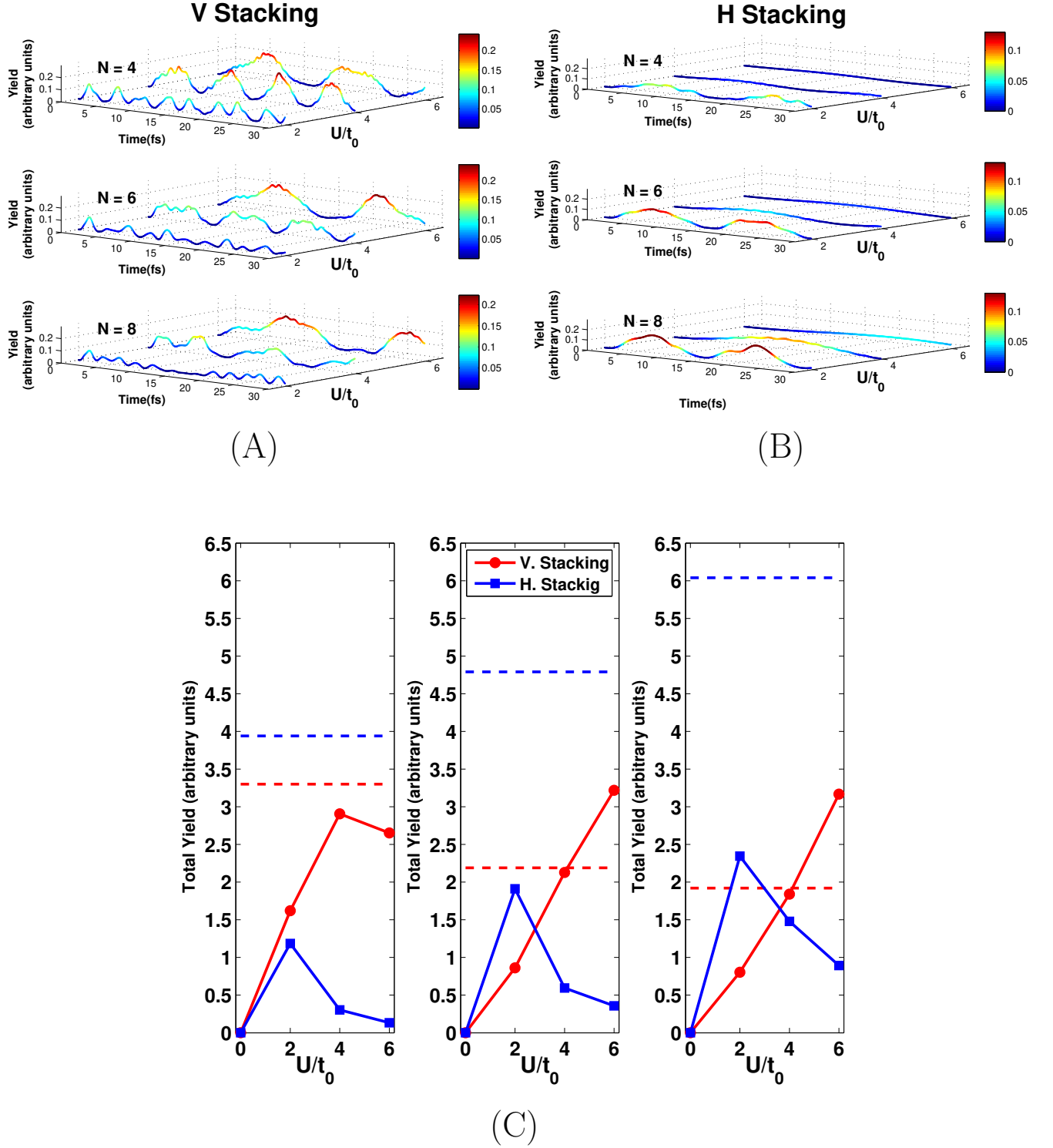


FIG. 5. (Color online) Time evolution profiles of different polyene dimers in V stacking ($t_{\perp} > 0$) (A) and H stacking ($t_{\perp} < 0$) (B) for different correlation strengths (U/t_0); here, $S_n \equiv 2^1A$ case is considered. Magnitude at each time step is also color coded as indicated in the adjacent colorbar. In (C), I^{total} is plotted as a function of correlation strength U/t_0 for $S_n \equiv 2^1A$. The left, center and right panels correspond to monomers of 4, 6 and 8 sites. Red filled circle corresponds to V stacking and blue filled square corresponds to H stacking. The broken lines in each panel correspond to the PPP values for unsubstituted system in V (red) and H (blue) stackings. The solid lines are given only as a guide to the eye.

TABLE III. Energy gaps in butadiene, hexatriene and octatetraene within Hückel, Hubbard and PPP models. Energy gaps are given in units of t_0 within Hückel and Hubbard models.

		$U/t_0 = 0$	$U/t_0 = 2$	$U/t_0 = 4$	$U/t_0 = 6$	PPP (eV)
butadiene	E_{1^1B}	1.40	2.19	3.40	4.94	5.83
	E_{2^1A}	2.33	2.06	1.54	1.17	5.34
	E_{T_1}	1.40	0.96	0.67	0.50	2.67
	$E_{1^1B} - 2E_{T_1}$	-1.40	0.27	2.06	3.94	0.49
	$E_{2^1A} - 2E_{T_1}$	-0.47	0.14	0.20	0.17	0.00
hexatriene	E_{1^1B}	1.07	1.68	2.78	4.26	5.05
	E_{2^1A}	1.81	1.63	1.25	0.96	4.36
	E_{T_1}	1.07	0.76	0.56	0.42	2.18
	$E_{1^1B} - 2E_{T_1}$	-1.07	0.16	1.66	3.42	0.69
	$E_{2^1A} - 2E_{T_1}$	-0.33	0.11	0.13	0.12	0.00
octatetraene	E_{1^1B}	0.88	1.39	2.44	3.90	4.56
	E_{2^1A}	1.47	1.37	1.07	0.83	3.75
	E_{T_1}	0.88	0.66	0.49	0.38	1.90
	$E_{1^1B} - 2E_{T_1}$	-0.88	0.07	1.46	3.14	0.76
	$E_{2^1A} - 2E_{T_1}$	-0.29	0.05	0.09	0.07	-0.05

suppressed.

In Table. I, we have also given the total yield when both X_\perp and t_\perp terms are included. It can be noted that X_\perp term differentiates the scenarios described by $t_\perp < 0$ (H stacking) and $t_\perp > 0$ (V stacking). In H stacking, the total yield is less than in the V stacking. Besides, I^{total} in H stacking decreases with increasing correlation strength while the opposite is observed in V stacking.

This behavior can be understood as follows: in H stacking ($t_\perp < 0$), the intermolecular bond order between corresponding sites i and i' on the two chains ($\langle E_{ii'} + E_{i'i} \rangle / 2$) increases while in $t_\perp > 0$ case it decreases as $t_\perp < 0$ favors delocalization of the electrons. Given that the bond orders follow this pattern, in the mean field limit, X_\perp contribution increases for higher bond orders. Thus the X_\perp term tends to homogenize the charge for H stacking as compared to V stacking. Hence, the intermediate ionic states are produced more easily in V stacking than in H stacking leading to greater singlet fission yield in V stacking. It can be observed from Fig. 4(B) that the resultant magnitude of the product of the overlap integrals ($\langle S_1 \otimes S_0 | \psi_i(0) \rangle$ and $\langle T_1 \otimes T_1 | \psi_i(0) \rangle$) are greater in V stacking than in H stacking. We can also expect similar behavior in the other large polyenes.

When $S_n \equiv 1^1B$, total yields are insignificant in both V and H stackings. Analysis employing full system Hamiltonian eigenstates shows highly disjoint overlaps with the initial and final states (Fig. 4(A)), similar to the Hückel calculations. Hence, only choice of 2^1A for the initial excited singlet state results in significant I^{total} in both stackings (Fig. 5).

The time evolution profiles, shown in Fig. 5(A) and 5(B) shed light on the dependence of I^{total} on monomer chain length in the Hubbard model. In V stacking, at a

particular U/t_0 , temporal variation of $I(t)$ in the evolution profile becomes weaker for longer chain systems, and the oscillatory pattern becomes more complex. In these cases, the eigenspectrum of dimers become more dense with increasing chain length and larger number of eigenstates contribute significantly towards $I(t)$. This leads to complex interference in the time evolution profile when the energies of the contributing dimer states are different. The time evolution profiles (Fig. 5(B)) also suggest that the significant eigenstates in H stacking are almost degenerate as the yield shows simpler time dependence. This can also be inferred from the right panel in Fig. 4(B), which shows that the contributing eigenstates have very nearly same energies.

3. Pariser-Parr-Pople (PPP) Model

Organic systems that we are interested in are semiconducting. Hence long-range interactions are not screened out as in metals and for a realistic modeling of the system we need to include explicit long-range electron-electron interactions. The PPP model with standard parameters is well suited for modeling conjugated organics^{51,58,67-69}. We have found that introducing long-range interaction dramatically changes the yield of triplets. When the wave packet is built from an optical state (1^1B) on one molecule and ground state on another, the total yield remains quite low for unsubstituted system in V stacking, although, the magnitude increases by several orders relative to the other two models. However, in H stacking the singlet fission yield is zero as in the Hubbard model. On the other hand, when the initial wave packet is constructed from 2^1A state and the ground state, there is

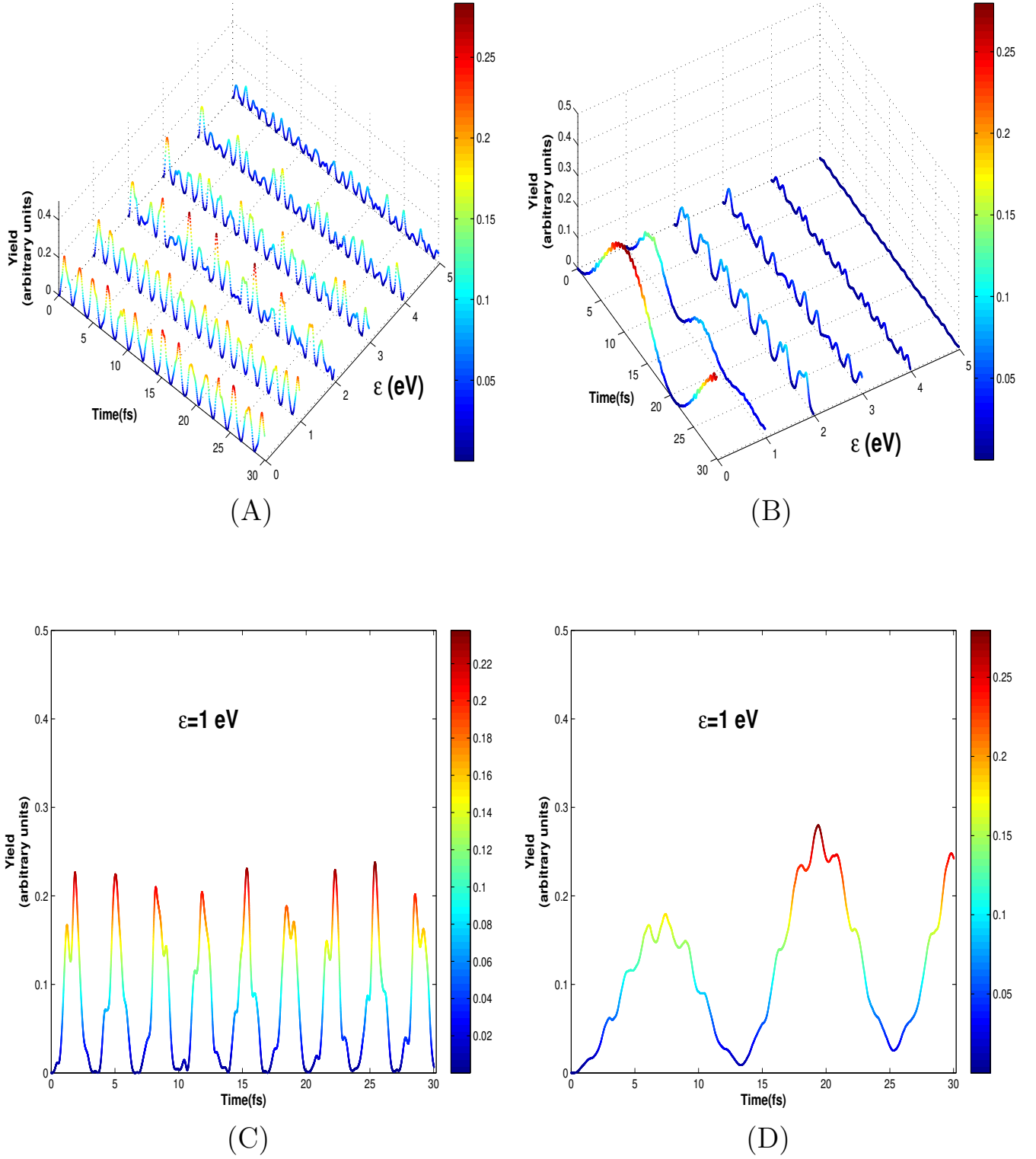


FIG. 6. (Color online) Yield as a function of time and donor-acceptor strength ϵ for singlet fission in 1,3-butadiene dimer from the lowest singlet excited state S_1 in (A) V stacking and (B) H stacking. For $\epsilon = 1$ eV, the yield from the optical singlet state is also shown in (C) V stacking and (D) H stacking. For $\epsilon \geq 2$ eV, we find that the lowest excited state is also the state with large transition dipole moment.

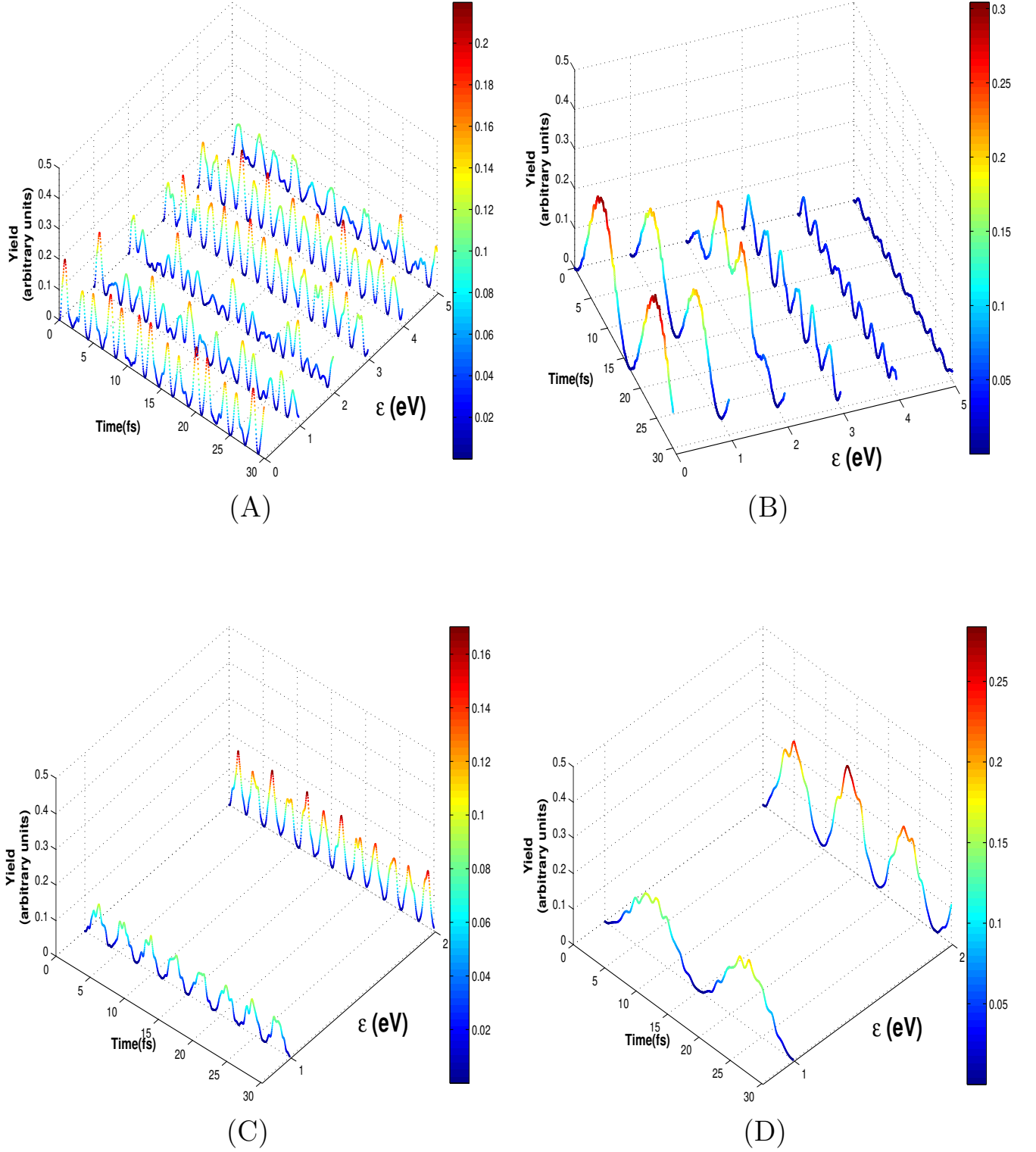


FIG. 7. (Color online) Yield as a function of time and donor-acceptor strength ϵ for singlet fission in 1,3,5-hexatriene dimer from the lowest singlet excited state S_1 in (A) V stacking and (B) H stacking. For $\epsilon = 1$ eV and 2 eV, the yield from the optical singlet state is also shown in (C) V stacking and (D) H stacking. For $\epsilon \geq 3$ eV, we find that the lowest excited state is also the state with large transition dipole moment.

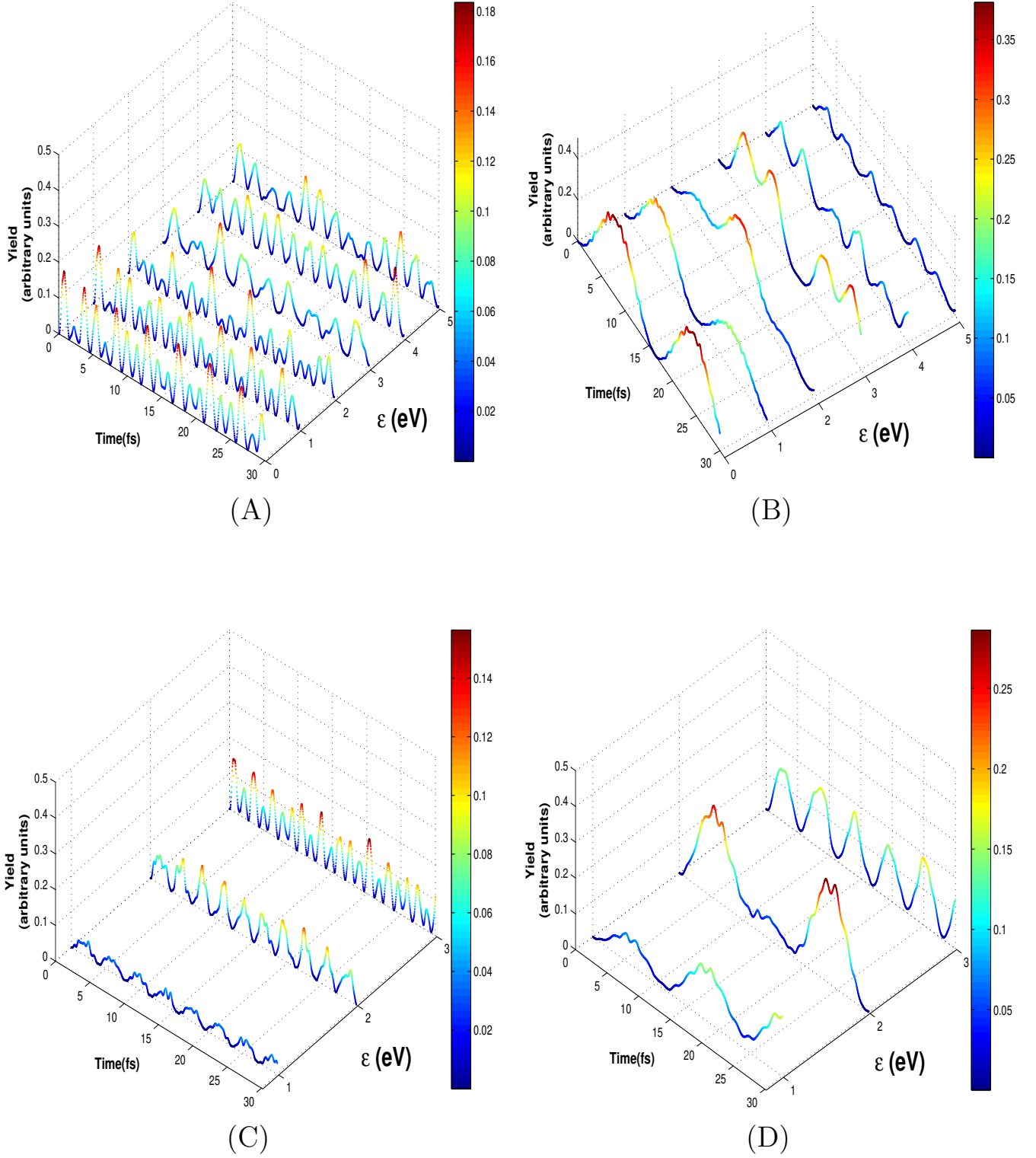


FIG. 8. (Color online) Yield as a function of time and donor-acceptor strength ϵ for singlet fission in 1,3,5,7-octatetraene dimer from the lowest singlet excited state S_1 in (A) V stacking and (B) H stacking. For $\epsilon = 1$ eV, 2 eV and 3 eV, the yield from the optical singlet state is also shown in (C) V stacking and (D) H stacking. For $\epsilon \geq 4$ eV, we find that the lowest excited state is also the state with large transition dipole moment.

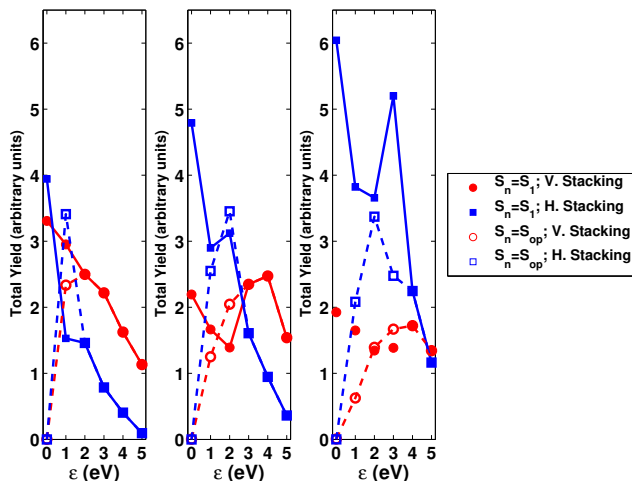


FIG. 9. (Color online) Total yield in unsubstituted and substituted polyene dimers are plotted as a function of substitution strength ϵ for both vertical and horizontal stacking orientations within the PPP model. The left, center and right panels correspond to monomers of 4, 6 and 8 sites. The color and symbol indices are given in the following and same in all three panels: red filled circle, $S_n \equiv S_1$, V stacking; blue filled square, $S_n \equiv S_1$, H stacking. The open symbols represent $S_n \equiv S_{op}$ scenarios in the corresponding systems. Beyond a certain ϵ , $S_n \equiv S_1 \equiv S_{op}$ and the curves coincide. The solid and broken lines are given only as a guide to the eyes.

significant increase in I^{total} , as can be seen from Figs. 5(C) and 9. In unsubstituted systems, large number of eigenstates have significant simultaneous projections on both $|2^1A \otimes 1^1A\rangle$ and $|T_1 \otimes T_1\rangle$; but these states are nearly isoenergetic in H stacking (Table. II) leading to constructive interference (Eq. 7) compared to V stacking in which there will be destructive interference (Fig. 6, 7 and 8).

The energy criteria proposed by Michl et al. (Ref. 6–8) that singlet fission is feasible when the initial state energy is almost identical with final state energy is seen to be operative in our model studies. In the Hückel model the optical state 1^1B is degenerate with the triplet state and as a consequence we have observed insignificant singlet fission yield. The 2^1A state in the Hückel model is also not isoenergetic with two triplets and hence 2^1A will also not yield singlet fission products.

When electron correlations are turned on, as in the Hubbard or PPP models, the triplet state comes down in energy as the lowest triplet state is a covalent state while the energy of 1^1B state, being ionic, increases. There is a crossover in the 1^1B and 2^1A states, depending upon the correlation strength and chain length^{68,70}. The 2^1A state remains nearly isoenergetic with twice of lowest triplet state energy (Table. III) and therefore an initial excited singlet in 2^1A state yields significant triplets in the singlet fission process. However, the 1^1B state is not isoenergetic with two triplets and yields insignificant final product.

Another important issue besides isoenergetic nature

is the ordering of the 2^1A and 1^1B states. In systems where 2^1A state lies below 1^1B state, the optical absorption gives large yield of the relatively long-lived 2^1A state due to internal conversion and we can expect significant fission yield. However, if the 2^1A state lies above the 1^1B state, the fission process will not have significant cross-section as the 1^1B state radiatively decays to the ground state; the 2^1A state in this case is only accessible through higher energy optical excitations. Thus, we can see that systems which are fluorescent will not yield triplets. Therefore, systems which are good for light emitting will not be good candidates for improving photovoltaic efficiency through singlet fission.

Effect of Donor-Acceptor Substitution

In unsubstituted polyenes, singlet fission has large cross-section to the $T_1 - T_1$ state only when the singlet state in the initial wave packet is 2^1A state. However, this state is optically dark and is weakly allowed since the electron-hole symmetry is not strictly held (electron-hole symmetry requires all sites to be equivalent). The optical state 1^1B , on the other hand has very small cross-section for singlet fission. Subsequently, substituted polyenes are choices for probing singlet fission in these systems as substitution breaks the electron-hole symmetry and makes the singlet state with the character of two triplets optically accessible.

The time evolution profiles for butadiene, hexatriene and octatetraene dimers for different substitution strength are shown in Fig. 6, 7 and 8 while the total yield for varying ϵ is plotted in Fig. 9. On donor-acceptor substitution, mixing of the one- and two-photon states take place which leads to different outcome in total yield. In V stacking, I^{total} decreases with increasing substitution strength when $S_n \equiv S_1$ and this outcome is independent of monomer size. Yet, when S_{op} , the state to which the transition dipole moment is largest is considered, non-monotonous behavior of I^{total} is observed with increasing ϵ . Thus, the total yield is dependent on the nature of the singlet excited state at small ϵ while at large ϵ the lowest excited singlet state is also the most strongly optically allowed singlet state and the distinction ceases. In contrast, H stacking orientation exhibits unique I^{total} profile with increasing ϵ (Fig. 9); large variation in I^{total} as a function of ϵ is observed for both $S_n \equiv S_1$ and $S_n \equiv S_{op}$ cases. This general trend is observable in all three polyene systems considered.

Full system Hamiltonian eigenstate analyses are performed for 1,4-substituted-1,3-butadiene with substituents of different strengths (Fig. 10); in this polyene system, beyond $\epsilon = 1.0$ eV, S_1 and S_{op} become identical. In V stacking, with increasing ϵ , larger number of eigenstates have significant projections with both initial and final coupled states, although, the product of the projections ($|\langle S_n \otimes S_0 | \psi_i \rangle \langle T_1 \otimes T_1 | \psi_i \rangle|$), becomes small for individual eigenstates. These eigenstates re-

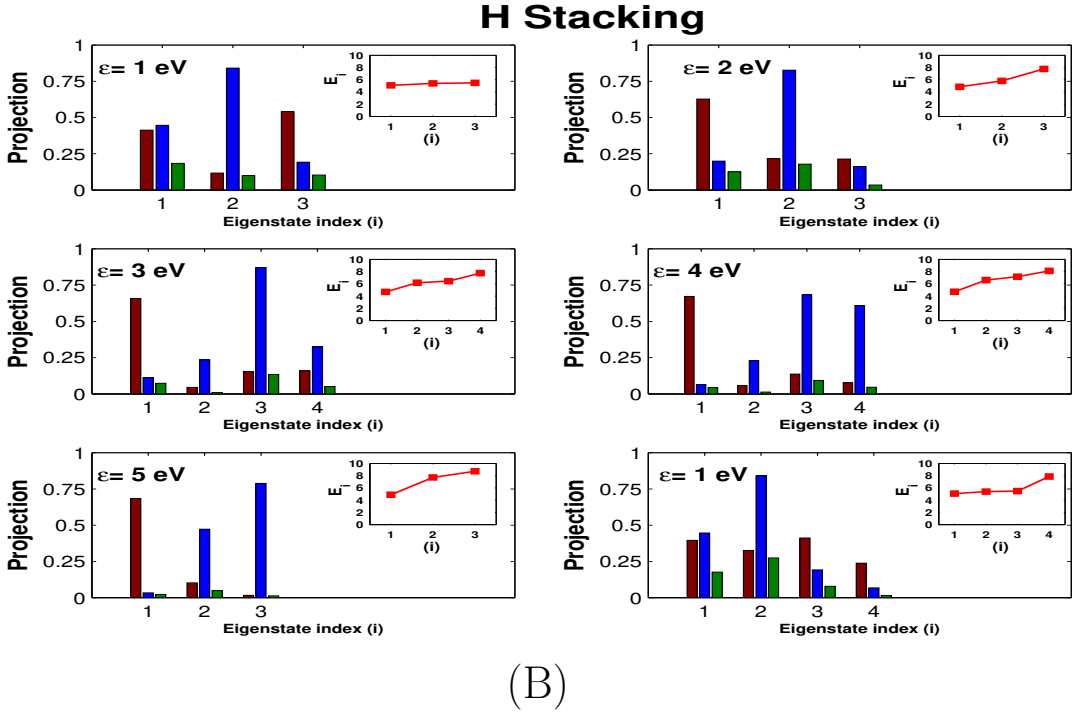
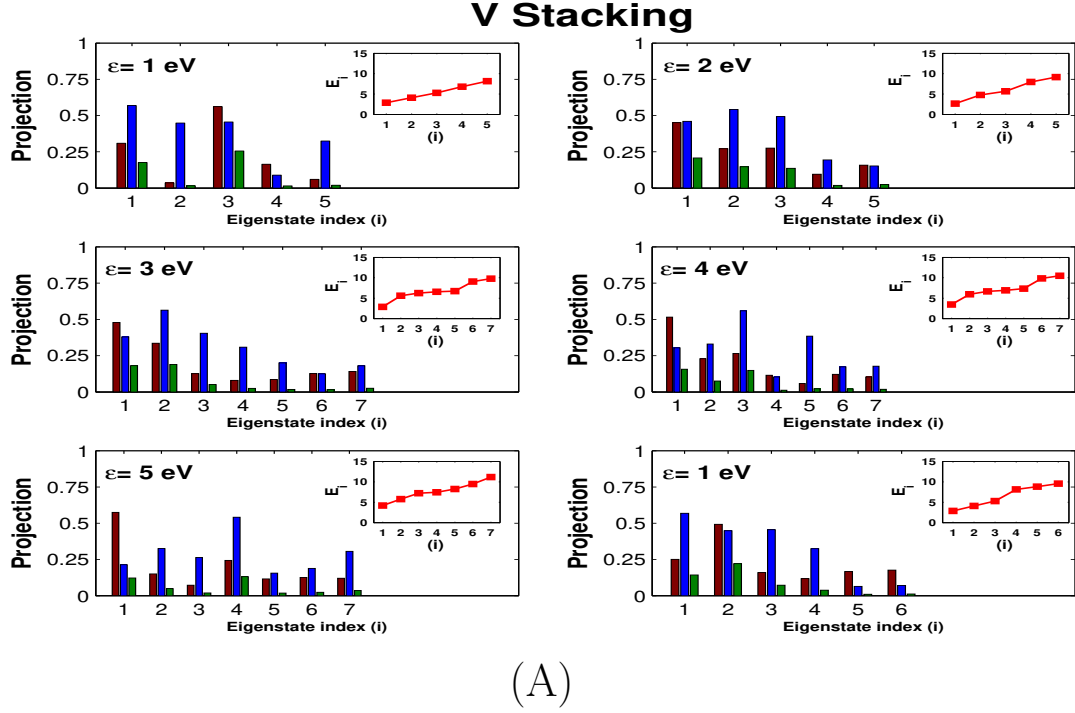


FIG. 10. (Color online) Significant projections of $S_n \otimes S_0$ and $T_1 \otimes T_1$ with full system eigenstates of the dimer within PPP model are shown (A) for the V stacking orientation and (B) for the H stacking orientation. In both sub-figures, the right bottom-most panel corresponds to initial state $|S_{op} \otimes S_0\rangle$ while the others correspond to $|S_1 \otimes S_0\rangle$. The color indices are same as in Fig. 4. Inset: E_i , the energy of the significant eigenstate 'i' as measured from the full system ground state is shown.

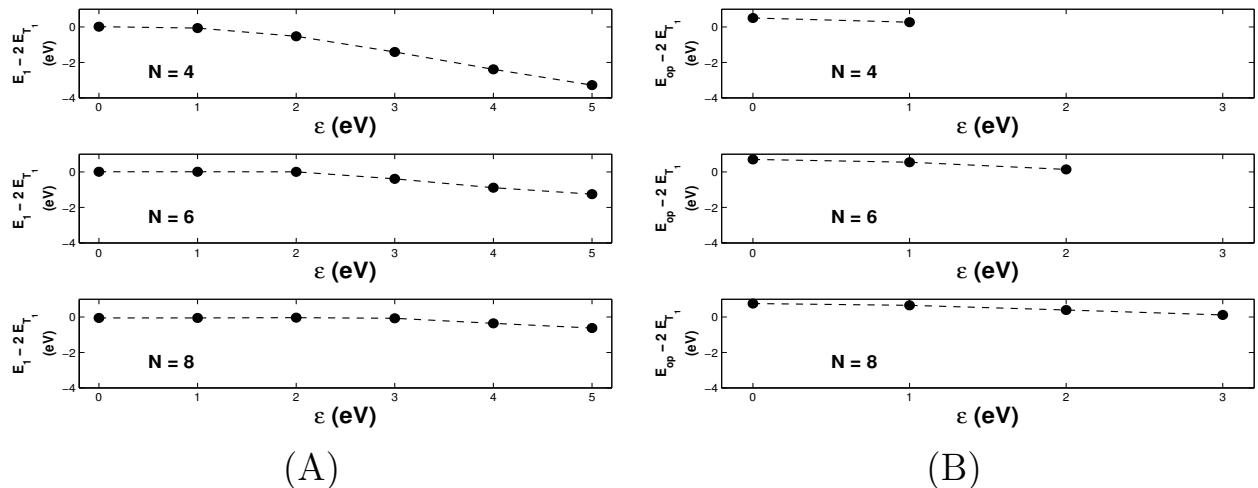


FIG. 11. Energy difference between the initial and final coupled states $[E_{S_n} - 2E_{T_1}]$ within PPP model are plotted against various ϵ . (A) corresponds to $S_N \equiv S_1$ while (B) correspond to $S_n \equiv S_{op}$ scenario. For $\epsilon = 0$, $S_1 \equiv 2^1A$ while S_{op} is the lowest energy state of B symmetry subspace ($S_{op} \equiv 1^1B$). In substituted PPP dimers, beyond a particular ϵ , S_1 becomes equivalent with S_{op} and shown in (A) only. The broken lines are shown only as a guide to the eyes.

main widely dispersed over energy eigenspectrum, which results in lower I^{total} . With $\epsilon = 1.0$ eV, total yield becomes smaller for $S_n \equiv S_{op}$ compared to $S_n \equiv S_1$, as the simultaneous projections associated with the important eigenstates are smaller in the former compared to latter (Fig. 10), even though, the distribution of the significant eigenstates in the eigenspectrum is similar in both cases. In the H stacking orientation the behavior differs significantly; the relevant eigenstates although remain isoenergetic for smaller ϵ ($\epsilon = 1.0$ eV and 2.0 eV), their simultaneous projection on to the coupled states get reduced significantly from the unsubstituted system. Higher dispersity in the eigenstates for larger ϵ values leads to further lowering of I^{total} . In the H stacking orientation, when $S_n \equiv S_{op}$ is considered, the total yield becomes higher compared to $S_n \equiv S_1$, as the simultaneous projections becomes significantly larger in this choice of S_n , contrary to the V stacking (Fig. 10(B)).

From our studies, we find that the donor-acceptor substitution plays an important role by mixing the S_1 and S_{op} states. The mixing results in the lowest energy state being simultaneously optically active and nearly of the same energy as of the final state of two triplets. The latter leads to large fission yield while the former makes this initial state optically accessible. The strength of ϵ required to maximize the yield is larger for longer systems although we cannot extrapolate it to the thermodynamic limit.

The energetics show that the singlet fission process is either slightly exoergic or endoergic for substituted PPP chains (Fig. 11(A) and 11(B)). The energetics consideration can be taken as a preliminary criterion, but overall yield in singlet fission will be governed by the evolution of the dimer under the influence of full system Hamiltonian. The endoergic process also results in significantly higher singlet fission products and may be due to inter-

chain interactions which are ignored in arriving at the energy criterion. This shows that following the dynamics of the evolution of the initial state under the full system Hamiltonian is important to assess the efficiency of singlet fission in real systems.

IV. CONCLUSION

We have studied singlet fission in polyene dimers using many-body quantum dynamics. The initial wave packet is a direct product of an excited singlet state on one polyene and ground state on the other. We have used exact wave packet dynamics to follow the coherent state, under the influence of the full Hamiltonian (H_{full}) which includes intermolecular interactions. In our study, correlated models are employed for individual polyenes and the intermolecular interaction consists of both transfer integral between corresponding sites in the two molecules and the site charge-bond charge repulsion integral which are comparable in magnitude. The time evolution is carried out using a predictor-corrector method with MSD4 scheme as predictor and fourth-order Adams-Moulton scheme as corrector. The total yield is the time-integrated projection of the evolved wavepacket on the desired final state.

For unsubstituted polyenes, we have found that the fission yield is high within Hubbard and PPP models when the excited state is 2^1A state while in the non-interacting model the fission yield is negligible. Analysis on butadiene dimer shows that in all models, the product of the overlap of the wave packet and the overlap of the final product state with the eigenstates of H_{full} is negligible when the wave packet is formed from 1^1B state. On the other hand, for wave packet constructed from 2^1A state, the product is significant for some eigen-

states. Another reason for higher magnitude of singlet fission yield in 2^1A case is the energetics, the 2^1A energy being very nearly equal twice the lowest triplet energy. In substituted polyene chains for small donor-acceptor strengths, singlet state derived from 1^1B state also gives significant fission yield within PPP model. For higher donor-acceptor strengths, the singlet state derived from the 2^1A state loses its two-triplet character and the fission yield goes down significantly. In the absence of push-pull groups, fission yield in an experiment is expected only when the 2^1A state lies below the 1^1B state. We also have found that fission yield depends on stacking geometry. In V stacking where the intermolecular transfer integral $t_{\perp} > 0$, the singlet fission yield in the PPP model decreases with increasing chain length while when $t_{\perp} < 0$ as in H stacking, there is an increase in fission yield.

ACKNOWLEDGMENTS

S.R. is thankful to the Department of Science and Technology, India for financial support through various grants. S.P. acknowledges CSIR India for a senior research fellowship. S.P. also thanks Prof. Diptiman Sen for financial support through his J. C. Bose fellowship.

- ¹W. Shockley and H. J. Queisser, *J. Appl. Phys.* **32**, 510 (1961).
- ²A. J. Nozik, M. C. Beard, J. M. Luther, M. Law, R. J. Ellingson, and J. C. Johnson, *Chem. Rev.* **110**, 6873 (2010).
- ³S. Singh, W. J. Jones, W. Siebrand, B. P. Stoicheff, and W. G. Schneider, *J. Chem. Phys.* **42**, 330 (1965); C. E. Swenberg and W. T. Stacy, *Chem. Phys. Lett.* **2**, 327 (1968); R. E. Merrifield, P. Avakian, and R. P. Groff, *ibid.* **3**, 386 (1969); R. P. Groff, P. Avakian, and R. E. Merrifield, *Phys. Rev. B* **1**, 815 (1970).
- ⁴P. M. Zimmerman, Z. Zhang, and C. B. Musgrave, *Nat. Chem.* **2**, 648 (2010).
- ⁵R. E. Merrifield, *J. Chem. Phys.* **48**, 4318 (1968); R. C. Johnson and R. E. Merrifield, *Phys. Rev. B* **1**, 896 (1970).
- ⁶M. B. Smith and J. Michl, *Chem. Rev.* **110**, 6891 (2010).
- ⁷J. C. Johnson, A. J. Nozik, and J. Michl, *Acc. Chem. Res.* **46**, 1290 (2013).
- ⁸M. B. Smith and J. Michl, *Annu. Rev. Phys. Chem.* **64**, 361 (2013).
- ⁹W.-L. Chan, M. Ligges, A. Jailaubekov, L. Kaake, L. Miaja-Avila, and X.-Y. Zhu, *Science* **334**, 1541 (2011).
- ¹⁰H. L. Stern, A. J. Musser, S. Gelin, P. Parkinson, L. M. Herz, M. J. Bruzek, J. Anthony, R. H. Friend, and B. J. Walker, *Proc. Natl. Acad. Sci. U.S.A.* **112**, 7656 (2015).
- ¹¹I. Paci, J. C. Johnson, X. Chen, G. Rana, D. Popović, D. E. David, A. J. Nozik, M. A. Ratner, and J. Michl, *J. Am. Chem. Soc.* **128**, 16546 (2006).
- ¹²E. C. Greyson, B. R. Stepp, X. Chen, A. F. Schwerin, I. Paci, M. B. Smith, A. Akdag, J. C. Johnson, A. J. Nozik, J. Michl, and M. A. Ratner, *J. Phys. Chem. B* **114**, 14223 (2010).
- ¹³T. Minami and M. Nakano, *J. Phys. Chem. Lett.* **3**, 145 (2012).
- ¹⁴T. Minami, S. Ito, and M. Nakano, *J. Phys. Chem. Lett.* **3**, 2719 (2012).
- ¹⁵T. Minami, S. Ito, and M. Nakano, *J. Phys. Chem. Lett.* **4**, 2133 (2013).
- ¹⁶E. C. Greyson, J. Vura-Weis, J. Michl, and M. A. Ratner, *J. Phys. Chem. B* **114**, 14168 (2010).
- ¹⁷P. E. Teichen and J. D. Eaves, *J. Phys. Chem. B* **116**, 11473 (2012).
- ¹⁸T. C. Berkelbach, M. S. Hybertsen, and D. R. Reichman, *J. Chem. Phys.* **138**, 114102 (2013); **138**, 114103 (2013).
- ¹⁹D. Casanova, *J. Chem. Theory Comput.* **10**, 324 (2014).
- ²⁰D. Beljonne, H. Yamagata, J. L. Brédas, F. C. Spano, and Y. Olivier, *Phys. Rev. Lett.* **110**, 226402 (2013).
- ²¹P. M. Zimmerman, F. Bell, D. Casanova, and M. Head-Gordon, *J. Am. Chem. Soc.* **133**, 19944 (2011).
- ²²P. M. Zimmerman, C. B. Musgrave, and M. Head-Gordon, *Acc. Chem. Res.* **46**, 13391347 (2012).
- ²³S. R. Yost, J. Lee, M. W. B. Wilson, T. Wu, D. P. McMahon, R. R. Parkhurst, N. J. Thompson, D. N. Congreve, A. Rao, K. Johnson, M. Y. Sfeir, M. G. Bawendi, T. M. Swager, R. H. Friend, M. A. Baldo, and T. V. Voorhis, *Nat. Chem.* **6**, 492 (2014).
- ²⁴A. J. Musser, M. Liebel, C. Schnedermann, T. Wende, T. B. Kehoe, A. Rao, and P. Kukura, *Nature Phys.* **11**, 352 (2015).
- ²⁵A. A. Bakulin, S. E. Morgan, T. B. Kehoe, M. W. B. Wilson, A. W. Chin, D. Zigmantas, D. Egorova, and A. Rao, *Nat. Chem.* **8**, 16 (2016).
- ²⁶X. Feng, A. V. Luzanov, and A. I. Krylov, *J. Phys. Chem. Lett.* **4**, 3845 (2013).
- ²⁷A. B. Kolomeisky, X. Feng, and A. I. Krylov, *J. Phys. Chem. C* **118**, 5188 (2014).
- ²⁸J. J. Burdett and C. J. Bardeen, *J. Am. Chem. Soc.* **134**, 8597 (2012).
- ²⁹J. J. Burdett and C. J. Bardeen, *Acc. Chem. Res.* **46**, 1312 (2013).
- ³⁰G. B. Piliand, J. J. Burdett, R. J. Dillon, and C. J. Bardeen, *J. Phys. Chem. Lett.* **5**, 2312 (2014).
- ³¹W.-L. Chan, M. Ligges, and X.-Y. Zhu, *Nat. Chem.* **4**, 840 (2012).
- ³²W.-L. Chan, J. R. Tritsch, and X.-Y. Zhu, *J. Am. Chem. Soc.* **134**, 18295 (2012).
- ³³W.-L. Chan, T. C. Berkelbach, M. R. Provor, N. R. Monahan, J. R. Tritsch, M. S. Hybertsen, D. R. Reichman, J. Gao, and X.-Y. Zhu, *Acc. Chem. Res.* **46**, 1321 (2013).
- ³⁴N. Renaud, P. A. Sherratt, and M. A. Ratner, *J. Phys. Chem. Lett.* **4**, 1065 (2013).
- ³⁵S. W. Eaton, L. E. Shoer, S. D. Karlen, S. M. Dyar, E. A. Margulies, B. S. Veldkamp, C. Raman, D. A. Hartzler, S. Savikhin, T. J. Marks, and M. R. Wasielewski, *J. Am. Chem. Soc.* **135**, 1470114712 (2013).
- ³⁶L. Wang, Y. Olivier, O. V. Prezhdo, and D. Beljonne, *J. Phys. Chem. Lett.* **5**, 3345 (2014).
- ³⁷N. Renaud and F. C. Grozema, *J. Phys. Chem. Lett.* **6**, 360 (2015).
- ³⁸B. J. Walker, A. J. Musser, D. Beljonne, and R. H. Friend, *Nat. Chem.* **5**, 1019 (2013).
- ³⁹J. Zirzmeier, D. Lehnher, P. B. Coto, E. T. Chernick, R. Casillas, B. S. Basel, M. Thoss, R. R. Tykwinski, and D. M. Guldi, *Proc. Natl. Acad. Sci. U.S.A.* **112**, 5325 (2013).
- ⁴⁰S. N. Sanders, E. Kumarasamy, A. B. Pun, M. T. Trinh, B. Choi, J. Xia, E. J. Taffet, J. Z. Low, J. R. Miller, X. Roy, X.-Y. Zhu, M. L. Steigerwald, M. Y. Sfeir, and L. M. Campos, *J. Am. Chem. Soc.* **137**, 8965 (2015).
- ⁴¹R. W. A. Havenith, H. D. de Gier, and R. Broer, *Mol. Phys.* **110**, 2445 (2012).
- ⁴²S. M. Parker, T. Seideman, M. A. Ratner, and T. Shiozaki, *J. Phys. Chem. C* **118**, 12700 (2014).
- ⁴³K. Aryanpour, A. Shukla, and S. Mazumdar, *J. Phys. Chem. C* **119**, 6966 (2015).
- ⁴⁴C. C. Gradinaru, J. T. M. Kennis, E. Papagiannakis, I. H. M. van Stokkum, R. J. Cogdell, G. R. Fleming, R. A. Niederman, and R. van Grondelle, *Proc. Natl. Sci. Acad. U.S.A.* **98**, 2364 (2001).
- ⁴⁵E. Papagiannakis, J. T. M. Kennis, I. H. M. van Stokkum, R. J. Cogdell, and R. van Grondelle, *Proc. Natl. Sci. Acad. U.S.A.* **99**, 6017 (2002).
- ⁴⁶C. Wang and M. J. Tauber, *J. Am. Chem. Soc.* **132**, 13988 (2010).
- ⁴⁷C. Wang, M. Angelella, C.-H. Kuo, and M. J. Tauber, *Proc.*

- SPIE **8459**, 845905 (2012).
- ⁴⁸R. J. Dillon, G. B. Piland, and C. J. Bardeen, J. Am. Chem. Soc. **135**, 17278 (2013).
- ⁴⁹A. J. Musser, M. Al-Hashimi, M. Maiuri, D. Brida, M. Heeney, G. Cerullo, R. H. Friend, and J. Clark, J. Am. Chem. Soc. **135**, 12747 (2013).
- ⁵⁰B. S. Hudson and B. E. Kohler, Chem. Phys. Lett. **14**, 299 (1972); K. Schulten and M. Karplus, **14**, 305 (1972).
- ⁵¹P. Tavan and K. Schulten, Phys. Rev. B **36**, 4337 (1987).
- ⁵²T. Zeng, N. Ananth, and R. Hoffmann, J. Am. Chem. Soc. **136**, 12638 (2014).
- ⁵³Y. Chen, L. Shen, and X. Li, J. Phys. Chem. A **118**, 5700 (2014).
- ⁵⁴E. Busby, J. Xia, Q. Wu, J. Z. Low, R. Song, J. R. Miller, X.-Y. Zhu, L. M. Campos, and M. Y. Sfeir, Nat. Mater. **14**, 426 (2015).
- ⁵⁵R. Pariser and R. G. Parr, J. Chem. Phys. **21**, 466 (1953).
- ⁵⁶J. A. Pople, Trans. Faraday Soc. **49**, 1375 (1953).
- ⁵⁷K. Ohno, Theor. Chim. Acta **2**, 219 (1964); G. Klopman, J. Am. Chem. Soc. **86**, 4550 (1964).
- ⁵⁸Z. G. Soos and S. Ramasesha, Phys. Rev. B **29**, 5410 (1984).
- ⁵⁹S. Ramasesha and Z. G. Soos, Int. J. Quan. Chem. **25**, 1003 (1984).
- ⁶⁰D. K. Campbell, J. T. Gammel, and E. Y. Loh, Jr, Phys. Rev. B **42**, 475 (1990); K. Tandon, S. Ramasesha, and S. Mazumdar, **67**, 045109 (2003).
- ⁶¹M. Wolfsberg and L. Helmholz, J. Chem. Phys. **20**, 837 (1952); R. Hoffmann and W. N. Lipscomb, **36**, 2179 (1962).
- ⁶²J. Crank and P. Nicolson, Mathematical Proceedings of the Cambridge Philosophical Society **43**, 50 (1947).
- ⁶³S. Ramasesha, J. Comput. Chem. **11**, 545 (1990).
- ⁶⁴T. Iitaka, Phys. Rev. E **49**, 4684 (1994).
- ⁶⁵S. C. Chapra and R. P. Canale, *Numerical Methods for Engineers*, 6th ed. (McGraw Hill Education (India) Pvt. Ltd., New Delhi, 2012).
- ⁶⁶I. I. Rabi, Phys. Rev. **51**, 652 (1937).
- ⁶⁷P. Tavan and K. Schulten, J. Chem. Phys. **70**, 5407 (1979); **70**, 5414 (1979); **85**, 6602 (1986).
- ⁶⁸Z. G. Soos, S. Ramasesha, and D. S. Galvão, Phys. Rev. Lett. **71**, 1609 (1993).
- ⁶⁹D. Baeriswyl, D. K. Campbell, and S. Mazumdar, *Conjugated Conducting Polymers*, edited by H. Kiess, Springer Series in Solid-State Sciences, Vol. 102 (Springer, Berlin, 1992).
- ⁷⁰Z. Shuai, J. L. Brédas, S. K. Pati, and S. Ramasesha, Phys. Rev. B **56**, 9298 (1997).